Doppler-corrected Balmer spectroscopy of Rydberg positronium

A. C. L. Jones,[*] T. H. Hisakado, H. J. Goldman, H. W. K. Tom, and A. P. Mills Jr.

Department of Physics and Astronomy, University of California, Riverside, California 92521, USA

D. B. Cassidy

University College London, London, United Kingdom

The production of long-lived Rydberg positronium (Ps) and correction for Doppler shifts in the excitation laser frequencies are crucial elements of proposed measurements of the gravitational freefall of antimatter and for precision measurements of the optical spectrum of Ps. Using a two-step optical transition via $2P$ levels, we have prepared Ps atoms in Rydberg states up to the term limit. The spectra are corrected for the first-order Doppler shift using measured velocities, and the Balmer transitions are resolved for $15 \leqslant n \leqslant 31$. The excitation signal amplitude begins to decrease for $n > 50$, consistent with the onset of motional electric field ionization in the 3.5-mT magnetic field at the Ps formation target.

I. INTRODUCTION

As a purely leptonic system, the metastable bound state between a positron and an electron, known as positronium (Ps), provides a valuable testbed for bound-state QED theory and tests of symmetries [1,2]. Ground-state triplet Ps has a mean lifetime of 142 ns for spontaneous annihilation, limiting the range of studies that can be performed. Excitation of Ps to states with $n > 2$ greatly reduces the annihilation rate, yielding lifetimes that are determined primarily by the rate of radiative decay to the ground state. The decay rates are a factor of 2 smaller than those of the hydrogen atom. The increase in lifetime resulting from excitation to Rydberg states makes possible a number of interesting experiments. For instance, Rydberg Ps has been proposed as a means of loading a stellarator, with the aim of creating a neutral positron-electron plasma [3]. It may be possible to improve the precision of $1S$-$2S$ measurements made using purely leptonic atoms such as Ps [4] or Mu [5] by using post excitation of the $2S$ states to long-lived, and readily ionized, Rydberg levels. Reconstructing the atom trajectories would then allow corrections for Doppler and transit time line-broadening effects [6]. As the various production mechanisms of Ps tend to favor high Ps velocities, Doppler effects must be corrected for or significantly reduced if precision measurements are to be conducted. Long-lived Rydberg Ps may also provide a path to searching for antigravity in antimatter [7] and may be of use for efficient production of antihydrogen through charge-exchange collisions [8–10]. Similarly, it may be possible to investigate positron or Ps bound states in molecules [11,12] or atoms [13–15] through charge-exchange collisions.

In this paper, we report progress in production of Rydberg Ps through a two-step optical excitation process, first via the $1S$-$2P$ (Lyman-α) transition at 243 nm and then via a Balmer transition from $2P$ to a Stark level with principal quantum number n. Narrow linewidths have been achieved via Doppler correction of measurements. This work builds on the earlier results of Ziock *et al.* [16] and Cassidy *et al.* [17], significantly

extending the range of excited states produced, with resonant bands resolved in n up to $\sim$ 30. Production of Rydberg Ps out to the term limit sheds light on the process of field ionization in a motionally induced electric field [18,19], highlighting the need for slow Ps atoms, even in experiments conducted in relatively weak magnetic fields. In addition to these applications, we outline a range of possible measurements that can be made and discuss improvements to the apparatus that will extend its capabilities.

II. EXPERIMENTAL DETAILS

A. Apparatus

1. Positron source

The experimental apparatus is similar to the one discussed in Refs. [17,20], with some key differences. Positrons are accumulated in a buffer gas Surko-trap [21] over $\sim$3-s intervals producing a pulsed beam with 5×10^4 positrons which are dumped in 5-ns-wide pulses at 0.3 Hz. Small numbers of positrons are used here as there is no accumulator in the present system to allow for efficient collection on longer time scales. The pulses have a spatial diameter of $\sim$3 mm in 0.08 T, yielding a beam diameter of $\sim$10–15 mm in the vicinity of the sample, where $B = 3.5$ or 6.9 mT. The lack of a HV pulsed accelerator or buncher, and the necessity of avoiding large electric fields in the vicinity of the target, mean that positrons are implanted into the material with energies over the range $170 \leqslant E \leqslant 190$ eV, due to the trap dumping procedure; this leads to incomplete thermalization of positrons within the target. As the positrons are not fully thermalized, some fraction of the Ps forms in excited states. Previous studies indicate a fraction of up to 2% of Ps is spontaneously formed in $n = 2$ states [22–26]. The excited-state Ps atoms thus formed are energetic and comprise a significant component of the background in the observed signal at early times (cf. discussion in Sec. II B for further detail). Positronium is produced by bombarding a clean p-type Si (100) target, heated to 900 K. Ps is produced efficiently by a process that leads to a nonthermal energy spread [27–29].

_____

[*]adric.jones@ucr.edu
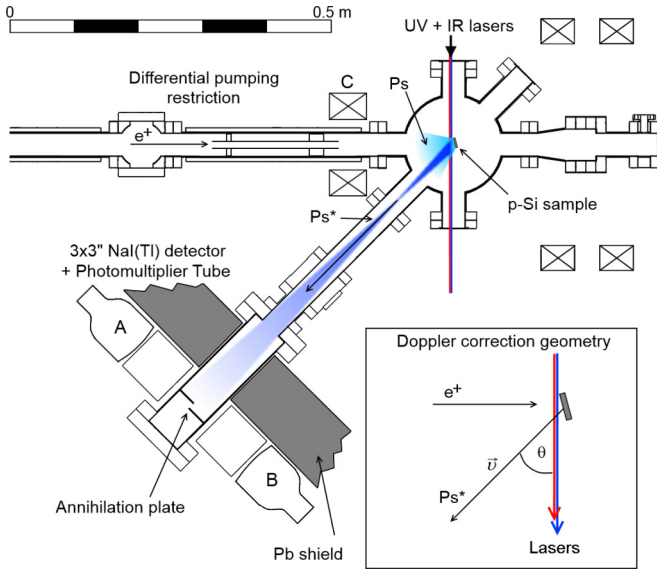
FIG. 1. (Color online) Schematic of the Rydberg Ps apparatus. Positron pulses are incident upon a clean *p*-Si target ($\sim 1.27 \times 1.42$ cm^2 surface area). Ps emitted from the sample is optically excited into Rydberg states (Ps*) via uv and ir laser pulses running transverse to the incident positrons. The sample is tilted at about $10°$–$15°$, in order to increase the signal (since Ps is preferentially emitted normal to the sample). Long-lived Ps traveling down the flight tube is detected via 511-keV annihilation γ's incident on 3×3 in. NaI (Tl) scintillators, coupled to photomultiplier tubes (A and B). The arrangement of detectors allows for either single-channel detection or coincident detection, which provides clear evidence of localized annihilation events.

2. Rydberg Ps production

In Fig. 1, the region of the apparatus relevant to the present experiment is shown. Positrons from the trap are implanted into the target in a 5-ns pulse, FWHM. The target is held at the center of a 6-in.-diameter chamber on a manipulator assembly, which provides *x*, *y*, *z*, and θ control. The experiments are conducted with typical operating pressures of 10^{-10}–10^{-9} Torr. The target is tilted approximately $10°$ toward the drift tube. Ideally the target would face the drift tube to maximize the Ps signal (which is anticipated to have some angular distribution, peaked for emission normal to the surface), however, as the lasers are introduced perpendicular to the positron beam a steeper angle would obstruct the path of the lasers, and/or result in a poor overlap of the expanding Ps cloud and laser pulses.

Positronium emitted at $45°$, with respect to the positron beam axis, can be detected at the end of the drift tube after colliding with a split steel plate (separated for pumping purposes by approximately 3 mm), upon which the positron annihilates via pickoff. During their flight to the target, Ps atoms experience a nonuniform magnetic field starting at 3.5 to 6.9 mT field at the target. This field drops off as the Ps leaves the target, first decreasing slightly before increasing by a factor of ~ 2 while passing coil C (see Fig. 1). Subsequently, the field in the rest frame of the Ps atoms decreases gradually to $< \sim 0.1$ mT. The slowly varying magnetic field between the target and detectors will lead to adiabatic evolution of the

Ps substates, which will remain in the original Stark manifold for $10 \lesssim n \lesssim 30$. For Ps with $n \gtrsim 30$, some n,m,l mixing will occur for the fastest atoms in the highest magnetic field regions [19]. We note that use of an electrostatic positron beam and magnetic shielding would eliminate the motional Stark effects. Detection of annihilation γ's is achieved via two 3×3-in. cylindrical NaI(Tl) detectors, coupled to photomultiplier tubes (PMTs). Detector A (see Fig. 1 for labeling) is attached to a Hamamatsu R2238 PMT, while B is coupled to an EMI 9821A. The detectors are situated outside of the vacuum chamber on opposing sides of the annihilation plate, with each covering a solid angle $d\omega/2\pi \approx 15\%$. This arrangement allows for coincident detection of the two 511-keV γ's emitted following Ps collisions with the plate. The detection of coincident pulses, as well as alternating measurements performed with and without the lasers, provide unambiguous evidence of long-lived Ps atoms.

3. Laser system

The laser light used in the present experiment is produced by two tunable dye lasers, pumped by a pulsed Continuum Surelite III Nd:YAG laser system. The fundamental output of the Surelite is an ir pulse at 1064 nm. Doubled and tripled light is also produced, at 532 nm ($\sim$50 mJ per pulse) and 355 nm ($\sim$200 mJ per pulse) respectively. The YAG is Q-switched via a TTL trigger that is a delayed copy of the pulse that triggers the positron trap dump, and so is fired at a typical rate of $\sim$0.3 Hz. Both triggers are synchronized to match the 10-Hz flash lamps that pump the YAG.

Exciting $1S$-$2P$ transitions requires uv pulses, centered about 243.05 nm. A coherent dye laser, with Coumarin LD489 dye, is pumped with the tripled YAG light, producing a blue pulse tuned to $\sim$485.8 nm, which is then doubled to yield a pulse (5 ns FWHM) at 242.9 nm. The light is detuned from the usual resonant peak for excitation from $1S$ to $2P$ to account for the typical Doppler shift of fast Ps atoms moving away from the laser pulse at a $\sim 45°$ angle, into the drift tube, as shown in the inset of Fig. 1. The uv pulse used in these experiments has a bandwidth of $\sim$100 GHz, and is intentionally made broad, by the use of the lowest order ($n = 1$) of the diffraction grating used in the dye laser, to maximize the excitation efficiency over a large spread of Ps velocities.

The ir pulse for the Balmer transitions is produced by a second coherent dye laser, pumped by the 50-mJ 532-nm pulse. The ir laser can be tuned over a range of $\pm \sim 15$ nm, from the peak output wavelength of a given dye. The wavelength range needed to excite Ps Balmer transitions to $n = 15$ and higher required two different dyes. A dye centered about 751 nm (LDS 751) was used for $n = 15 \rightarrow \sim 25$ while a second dye, centered about 722 nm (LDS 722), covered the remaining range to just beyond the term limit at $\sim$729 nm. The ir dye laser was tuned to the highest order accessible ($n = 4$) to reduce the bandwidth of the laser to $\sim$50 GHz.

A small fraction ($\sim 1\%$) of each pulse was split off from the ir laser, and redirected into a Bristol 821 Wavemeter on each shot, yielding a measure of the laser line center vacuum wavelength. Given the large bandwidth of the ir pulse, and the wavemeter's free spectral range $\sim$45 GHz, the precision of the wavemeter is specified to be ±0.2 cm^{-1} (or ±0.01 nm)

under these conditions [30]. In practice, wavelengths for a
particular scan are found from a second-order polynomial fit
to the wavemeter output as a function of dye laser grating
position. Nevertheless, the precision of our resolved Balmer
line centers is limited by wavelength measurement offsets of
∼0.07 nm, due to the bimodal profile of the ir laser [31]. For
most of the scans, the offset had a fixed, but undetermined,
value. For other scans (Fig. 3 being the only data presented
here to which this applies), the offsets appeared as periodic
0.07-nm steps (separated by ∼0.18 nm) in each individual
scan. However, this problem did not affect the measured line
shapes due to the use of the second-order polynomial fit to
represent the measured wavelengths.

The two dye lasers are directed out of a temperature-
controlled (±1 °C) laser enclosure through a small opening,
before alignment into the target chamber. The geometry of
the experiment constrains the incident angle of the beams
such that they are introduced near the edge of the window (a
uv-grade fused-silica port in a 2.75-in CF flange). Alignment
is facilitated by observing the relative positions of the beam
and Ps target at the exit window (see Fig. 1).

B. Data analysis

Analysis of the data is performed offline. Digital oscillo-
scope (Agilent 54855A DSO) traces of the voltage output of
the two PMTs are recorded, as a function of time after the
positron pulse hits the sample, at a sampling rate of 1 GSa/s.
The first step in the analysis involves converting pulses in
the scope traces into counts, recorded as a function of time.
Absolute timing is achieved by triggering the oscilloscope
using the digital trigger pulse that dumps the positron pulse
from the trap and fires the laser.

Pulses from the NaI(Tl) scintillators have rise times
∼100 ns from base to peak, followed by a relaxation over
∼200 ns. As such, to resolve pulses occurring within ∼200 ns
of each other, it is necessary to reduce the long decay tail
of the pulses. Pulse traces are narrowed in code by adding a
scaled, inverted, copy of the signal, shifted forward in time
($t' = t + 75$ ns). This operation converts the broad (∼250 ns)
asymmetric pulse shape to narrow Gaussian-type features with
a width of ∼100 ns (FWHM). The time of detection is subse-
quently determined by finding the rising edge of the pulse at a
threshold of 5 meV, compared to typical 511-keV pulse heights
of ∼100 meV. Using this procedure, detection times can be re-
solved to an accuracy of ∼10 ns, while the pulse pair resolution
is ∼150 ns.

In Fig. 2, typical data, plotted as a function of the Ps time
of flight (TOF), are presented. The data of Fig. 2 constitute
evidence that Ps is being excited to states with principal
quantum numbers in the range $n = 15$ to 17, which can
survive up to 5 μs and travel over a 0.5-m path to annihilate
upon impact with a metal plate. In Fig. 2(a), the existence of
long-lived Rydberg Ps is demonstrated by comparison of the
observed count rate with and without laser excitation. The data
were collected in two scans over the course of ∼31 h. During
these experiments, the ir laser was scanned within the range
738.7 to 743 nm which, due to the Doppler effect and the
distribution of Ps energies, primarily results in excitation of
Ps atoms to final states of principal quantum number $n = 15$
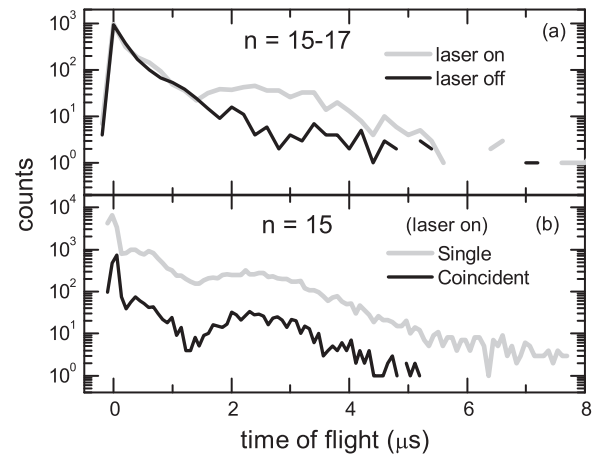
FIG. 2. (a) Comparison of observed two detector singles count
rate with (gray line) and without (black line) laser excitation of Ps
in the region of the time-of-flight (TOF) spectra corresponding to
Rydberg Ps. The data here comprise ∼5300 shots in total, collected
over a period of ∼31 h while scanning the ir laser through the range
∼738.7 to 743.0 nm. (b) Comparison of the signal due to the sum of
single-channel detections (gray line) and that due only to coincident
detection of annihilation γ's (black line). Here, the data were collected
in a single scan of 16 800 shots, with the ir repeatedly scanned across
the $n = 15$ resonance from 741.3 to 742.6 nm. In both plots, data are
normalized to yield the count rate per 1000 shots, in 0.2-μs TOF bins.
Since the ir wavelength was scanned through the resonance during
these measurements, the count rate with the laser fixed on resonance
would be ∼50% higher.

to 16. A large increase in the signal is observed between 1.5
to 6 μs when the lasers are fired ∼10 ns after the emission
of Ps from the target. In Fig. 2(b), the sum of the signals
from the two detectors is compared with the signal due to
2γ coincident detection of Ps. The coincident signal clearly
enhances the Rydberg Ps signal with respect to background,
demonstrating that we are detecting Ps in the vicinity of the
detectors, delayed up to 8 μs. Here, the data were collected in
a single scan of 16 800 shots, with the IR laser scanned across
the $n = 15$ resonance in the range 741.3 to 742.6 nm. The
peak in the TOF data in the range of 0.2–1.2 μs is attributed
to spontaneous emission of fast Ps in excited states. Although
the coincident signal has a significantly reduced background,
the data collection rate is reduced by a factor of ∼20, and so
the combined single-channel data are used instead.

The observed background signal comprises at least three
components. Although not shown in full in the schematic
(Fig. 1), there is substantial lead shielding around the two
detectors, particularly in the space between the detectors and
the main chamber. Nonetheless, 1-2 prompt ($0 \leqslant t \leqslant 50$ ns)
annihilation γ's, on average, are detected on each shot due to
annihilation in the vicinity of the target. This signal, which
should be proportional to the incident positron pulse, provides
a means of cross calibrating data sets. A second background
component is also observed, producing a shoulder on the
prompt peak, plateauing around 500–600 ns. While it is
possible for energetic ground-state ortho-Ps to survive the
flight to the detector, the observed shoulder in the data would
imply a population of epithermal ground-state Ps that exceeds

the magnitude of the incident positron pulses. Assuming that the signal is due to epithermal 2^3S Ps on the other hand suggests a small fraction of the Ps atoms are produced in excited states, comparable to the fraction of excited-state Ps observed in previous experiments [25,26]. Due to their large velocity, these epithermal atoms (with a mean energy of ~2.5 eV) will have minimal overlap with the laser pulses. Finally, detection of annihilation radiation from spontaneous annihilation of ground-state ortho-Ps in flight (reached through radiative decay of Rydberg Ps, prior to the atom reaching the annihilation plate) may contribute to the observed signal, particularly as the Ps approaches the end of the tube. This effect will be most significant for short-lived states, with the magnitude of the contribution dependent on the lifetime of the Rydberg states. With a lifetime on the order of ~3 μs, decay in flight could account for ~20% of the observed signal, and thus produce a systematic overestimation of the flight distance and Ps velocity, resulting in a skewed broadening of Doppler-corrected lineshapes. A lack of clear evidence for this effect is thus suggestive of radiative decay lifetimes in excess of the typical flight times observed.

In Fig. 3(a), the delayed annihilation counts (indicated by the shading scale, white being zero counts, black being the maximum number of counts in any data bin) detected over the course of a 17-h run (consisting of 16 800 Ps shots) are shown as function of Ps TOF, t and ir laser wavelength, λ in the vicinity of the transition from the 2^3P manifold to a final state of $n = 15$. The dark curved band between 741.5 and 742 nm is due to the resonant excitation of Ps and occurs over a range of wavelengths due to the Doppler shift of the laser light in the rest frame of the Ps atoms. In order to accurately determine the lineshape and center of a resonance, the ir wavelength must be corrected for the Doppler shift. The magnitude of the shift is a function of Ps velocity in the direction of the laser pulse and can be derived from the TOF t,

$$v_\perp = \frac{d}{t}\cos\theta, \tag{1}$$

where θ is the angle between the Rydberg Ps atoms trajectory and the laser beam and $d = 0.56$ m is the length of the flight path from the sample to the annihilation plate. The typical velocity of Ps atoms emitted from the Si sample is $\sim 10^5$ m s^{-1}, and so the Doppler correction applied is nonrelativistic. The effective wavelength λ' as observed by a given Ps atom is, to first order,

$$\lambda' = \lambda\left(1 + \frac{d}{tc}\cos\theta\right), \tag{2}$$

where c is the speed of light. The typical magnitude of the Doppler correction is thus ≤ 0.5 nm or less in the present experiment. In Fig. 3(b), the data of Fig. 3(a) are plotted versus the Doppler-corrected wavelength λ'. The correction applied assumes both a point source of Ps, and a well-defined distance of travel. Together, these assumptions result in the neglect of a small contribution to the width of the observed resonance after Doppler correction, on the order of 0.05 nm out of a total width of 0.2–0.25 nm. The other significant contributions to the observed width are due to the ir laser bandwidth and a splitting of the levels due to the motional Stark effect, which is dependent on the Ps atoms' velocity component
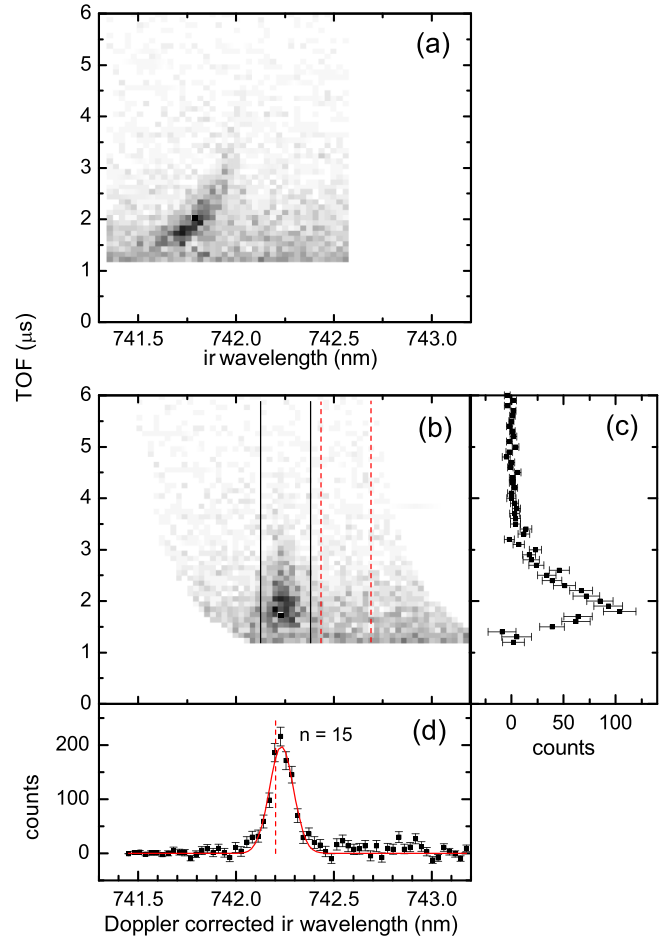
FIG. 3. (Color online) Data are presented in plots (a)–(d) for resonant excitation of Rydberg Ps to Stark manifold of states with principal quantum number $n = 15$, taken over a scan of 40 wavelengths (before Doppler correction), with 500 shots per wavelength. In plot (a), detection events are shown as a function of TOF and ir wavelength; the number of detected counts is indicated by the intensity scale, with black being maximum, (b) Doppler-corrected data, (c) a selection of the data of plot (b) summed over delays from 1.2–6 μs, to yield counts as a function of TOF, (d) data of plot (b) are projected to yield counts as a function of Doppler-corrected ir wavelength. A Gaussian fit yields the resonance center and width. Full details of the data analysis methods are given in the text.

transverse to the magnetic field and broadens with increasing principal level n. For $m = 0$, the Stark splitting increases like $n(n-1)$ [18].

In Fig. 3(c), the Doppler-corrected data are projected, by summing over a range of wavelengths, to produce a TOF time distribution for the $n = 15$ Rydberg level. Here, the background count rate is accounted for by subtraction of an equivalent selection of adjacent data, as indicated by the solid and dashed vertical lines on Fig. 3(b). The data here effectively represent counts per 4500 shots, assuming the Doppler correction does not significantly distort the proportion of data in equally sized wavelength bins.

Finally, in Fig. 3(d), the data are projected by summing over all TOF times greater than 1.2 μs, to produce a spectrum

of counts as a function of Doppler-corrected wavelength. In the vicinity of the peak, the signal rate is effectively counts per 500 shots. The background subtraction is performed by scaling a TOF distribution curve in which no Rydberg Ps is generated, to the prompt peak of the signal and subtracting this curve from each wavelength slice of the raw data, prior to applying the Doppler correction [32]. A Gaussian fit provides a measure of the resonant transition wavelengths, as well as the width of observed features. Here, the measured line center is 742.232 ± 0.004 nm (statistical) ± 0.07 nm (systematic), in reasonable accord with the expected transition center at 742.202 nm. The measured line is 0.145 ± 0.009 nm wide (FWHM), primarily due to the ir laser bandwidth.

III. RESULTS AND DISCUSSION

A. Lifetime measurements

Measurements of the mean lifetime τ of a given Rydberg level can, in principle, be derived from TOF spectra. The expected distribution of counts as a function of time of flight depends on two factors: the velocity distribution of Ps emitted from the target and the lifetime of the state of Ps. The observed distribution of counts as a function of time $N(t)$ is given by

$$N(t) = N_0(v) \exp\left(\frac{-d}{v\tau}\right). \tag{3}$$

If the lifetime of a given state is sufficiently long, very little loss is expected as a function of flight time, and so the exponential term can be neglected, leaving only the Ps velocity distribution term $N_0(v)$ (for sufficiently high n, thermal photoionization should be considered [33]). Taking the ratio of the TOF distribution of an exponentially decaying state to that of a relatively long-lived state should thus return an exponential decay, dependent only on the lifetime of the shorter-lived state.

To avoid sensitivity to background, it is preferable to find the difference in the decay rates of two states, $\Gamma \equiv 1/\tau_1 - 1/\tau_2$, by finding the best fit of a long-lifetime data set to a shorter-lived-state data set multiplied by an exponential function $e^{\Gamma t}$.

In Fig. 4, the area normalized TOF spectra of Rydberg Ps in the $n = 15$ and 20 states are compared. The result of a least-squares-fitting routine yields a difference rate of $\Gamma = (0.01^{+0.20}_{-0.01})\ \mu\mathrm{s}^{-1}$. The data are not precise enough to detect any difference between the two lifetimes. Were the Rydberg Ps prepared in a field-free environment, $n^3 D$ states would primarily be excited, yielding an expected lifetime difference of $\sim 0.2\ \mu\mathrm{s}^{-1}$ [34], which is also consistent with the measured value. However, as the Rydberg Ps atoms are created in a motionally induced electric field, the Stark splitting of states becomes an important consideration. As such, we might expect mean lifetimes associated with higher-l states ($\sim 100\ \mu\mathrm{s}$) [35,36]. A more definitive result could be obtained with a slower source of Ps, or a longer flight tube.

The observed peak in the TOF distributions is at $\sim 1.7\ \mu\mathrm{s}$. The Ps kinetic energy at this TOF is ~ 0.6 eV. The peak in the Ps energy distribution will be slightly less than 0.6 eV, due to the inverse relationship between the TOF and energy.
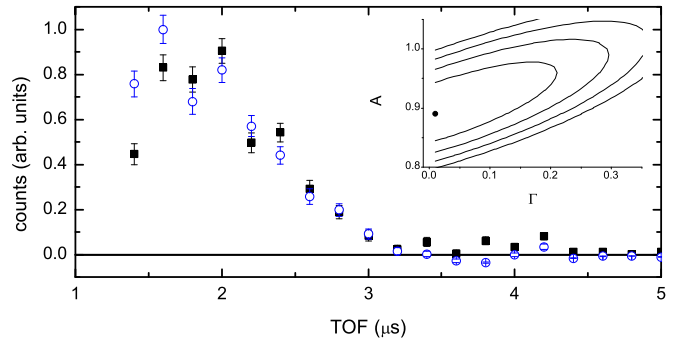
FIG. 4. (Color online) Comparison of the TOF spectra of Ps for $n = 15$ (solid squares) and $n = 20$ (open circles) resonances. Inset is a contour plot of the χ^2 distribution as a function of the fit parameters A and Γ, with the minimum value indicated by the black spot. At the level of 1σ uncertainty, the observed minimum is consistent with both the expected difference rate ($0.2\ \mu\mathrm{s}^{-1}$) and with no difference between the lifetimes of the states.

B. Ps energy spectrum

The energy spectrum of Ps emitted from a Si target is of interest due to the nonthermal process of Ps production [27,28]. A number of groups have investigated Ps kinetic energies, using a variety of techniques, each with its own advantages and limitations (see for example Refs. [37–40]). In the present experiment, Ps kinetic energies are determined directly from the measured TOF of individual Ps atoms that have been excited to long-lived Rydberg states, collected over a small angular range of emission. The long flight times seen in the present experiment allow for high-precision measurements of the Ps kinetic energies.

In Figs. 5(a) and 5(b), detected counts are sorted by kinetic energy ($E = \frac{1}{2}md^2t^{-2}$, where t is the time of flight, m is the Ps mass, and d is the flight path) and the Doppler-corrected ir wavelength for measurements about $n = 20$ and 15, respectively. The data are then summed over bands of ir wavelength about the resonance, with a background subtracted from an equal adjacent band off resonance. The summed regions are indicated on plots (a) and (b) by dashed horizontal lines. In plot (c), the two sets of data are summed together to yield the energy spectrum.

As the Rydberg Ps is formed in a (motionally induced) electric field, we expect the lifetimes may greatly exceed even the longest flight times observed in the present experiment. No correction is made here for loss due to radiative decay. If the lifetimes are shorter than anticipated, the correction would increase the apparent proportion of slow Ps.

A source of thermal Ps atoms, held at a temperature of ~ 1000 K (i.e., the temperature of the present Ps target), would yield a mean energy of ~ 0.1 eV. Here, we observe an average Ps energy of ~ 0.4 eV, far in excess of the thermal value. The proposed mechanism for Ps production in Si [27] is not expected to produce a thermal spread of energies, although the expected mean energy ~ 0.16 eV is more in line with the thermal value than that observed here. The broad Ps energy spectrum observed here is thought to be at least partially the result of incomplete thermalization of the incident positron beam, which is implanted with a mean energy of just 180 eV.
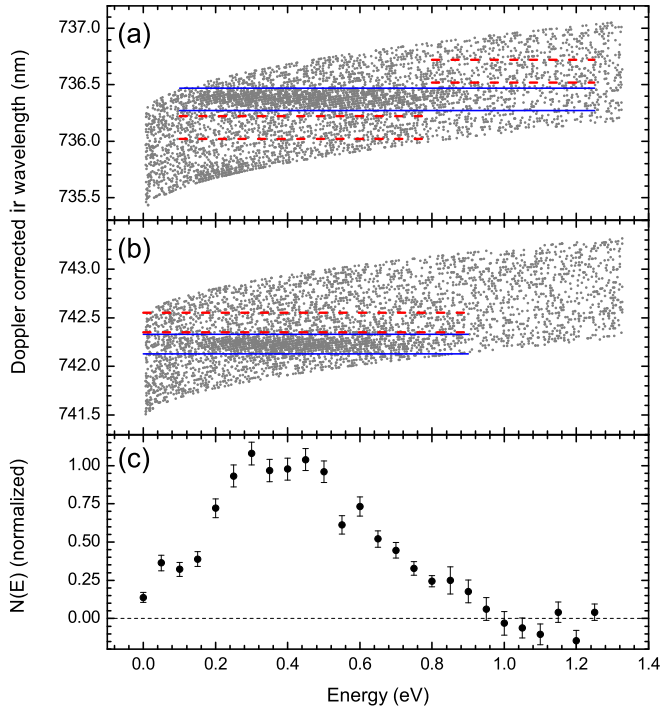
FIG. 5. (Color online) The energy spectrum of Ps emitted from the *p*-Si sample is found by first sorting the observed counts by the Doppler-corrected ir wavelength and Ps kinetic energy. Sorted data are shown in (a) for $n = 20$ and (b) $n = 15$. In (c), the averaged energy spectrum of plots (a) and (b) is given. The individual spectra are found by binning the data within the wavelength bands indicated by solid horizontal lines and subtracting a background signal obtained similarly from the regions indicated by dashed horizontal lines.

In contrast, the implantation energy required to prevent half of the implanted positrons from being reemitted is approximately 3 keV. A more complete study of the Ps energy spread from Si will require implantation energies on the order of 1 keV. This could not be achieved with the apparatus described here, as the only means of varying positron implantation energy was to apply a potential to the target, and electric fields on the order of ∼1 kV cm⁻¹ are sufficient to field ionize Rydberg states of $n \geqslant 20$.

C. Rydberg spectroscopy

Although Balmer resonances from $n = 15$–30 are easily observed with our apparatus, the precision of the resolved line centers is limited by the aforementioned periodic wavelength measurement offsets of 0.07 nm, due to the bimodal profile of the ir laser [31]. This effect could be eliminated by reducing the ir linewidth with an intracavity etalon to better match the wavemeter specifications, and/or seeding the dye laser to achieve single-mode operation.

Correction of the Doppler effect is only necessary due to the angle of the laser pulse with respect to the time-of-flight apparatus, as illustrated in the inset of Fig. 1. In the future, the target chamber will be reconfigured to allow for laser access perpendicular to the velocity of the detected Ps. The Doppler correction rests on the approximation of a point source of Ps, and ignores the finite angular acceptance of the drift

tube. Better accuracy could be achieved by focusing positrons onto the target, along with position-sensitive detecting of the Rydberg atoms. Resonances could also be further narrowed by reduction of the angular acceptance of the apparatus, and by reducing the magnetic field in the vicinity of the target, although both measures come at the cost of signal rate.

D. Measurements at the term limit and field ionization

The magnetic field at the target is oriented along the axis of the positron beamline; the observed Ps atoms are emitted at a $45°$ angle with respect to this axis and as such experience an electric field in their rest frames. The motional electric field splits the excited Rydberg state into $n - 1$ evenly spaced levels (to first order), characterized by the parabolic quantum number $-(n - 1) < k < (n - 1)$. As such, the splitting is proportional to both the Rydberg level n and the magnitude of the electric field at the target ($|\overrightarrow{\mathbf{E}}| = |\overrightarrow{\mathbf{v}} \times \overrightarrow{\mathbf{B}}|$), where excitation occurs. For small $\overrightarrow{\mathbf{v}}$, the energy levels are given by Hogan [18] as

$$E_k = \tfrac{3}{2} e a_{\mathrm{Ps}} n k |\overrightarrow{\mathbf{E}}|, \tag{4}$$

where $a_{\mathrm{Ps}} = 2a_B$ is the Ps Bohr radius. The total broadening due to the splitting is thus

$$\Delta E_k = 3 e a_B n (n - 1) |\overrightarrow{\mathbf{E}}|. \tag{5}$$

In the present experiment, the average velocity of Ps atoms is about 2×10^5 m s⁻¹. The expected range of the Stark splitting at $n = 25$ with a magnetic field at the target of 3.5 mT is 0.0227 nm total, and thus with an expected RMS width (uncertain due to the unknown population of k states in the present experiment) on the order of ∼0.01 nm, a factor of ∼4 smaller than the width of the ir laser.

In Fig. 6, measurements of the observed count rate are displayed as a function of Doppler-corrected ir wavelength
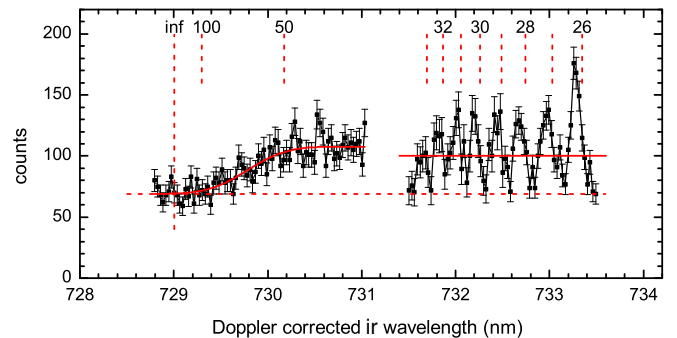
FIG. 6. (Color online) Behavior of the observed resonant excitation of Ps in the vicinity of the term limit. Comparison of the apparent efficiency of production of long-lived atoms as a function of magnetic field strength at the point of excitation is demonstrative of field ionization resulting from the motional Stark effect. Dashed vertical lines indicate expected positions of resonances, converging on the term limit at $n = $ inf. A dashed horizontal line at ∼70 counts indicates the apparent background signal. The solid horizontal line through the resolved peaks indicates the mean value, which agrees well with the observed signal in the region of $n = 50$ where peaks are no longer resolved. A solid line through the data (a fitted error function) from 731 to 729 nm provides a visual guide to illustrate the trend in the signal due to field ionization.

covering a range that extends from the highest resolved resonant transitions up to the term limit. Data are contributed from four separate experimental runs, with an equal number of scans performed in each run, such that there are ~420 Ps shots per wavelength. Across these scans, the only significant change was a slowly diminishing laser fluence due to the decay of the YAG flash lamps and laser dyes. To avoid producing artifacts in the data, no background has been subtracted here. An extrapolation of the mean count rate for wavelengths less than 729 nm, however, lies in close agreement with the minima between the resolved resonances for wavelengths greater than 732 nm. For three of the data sets, the change is small and appears to have little effect on the observed transition efficiency. For the fourth data set, covering the range from $n = 31$ to 33, the observed signal appeared to be smaller than anticipated. The data, above the background level, have been rescaled by a factor of 1.3. This scaling factor was found by fitting a series of Gaussian peaks to the resolved data (from $n = 26$ to 33), with a step function of variable height at the transition between sets. The rescaling factor found through this procedure is of comparable magnitude to the decrease in laser fluence between the two data sets, which was an average decay of ~15% in the uv and ir lasers. Rydberg Ps production was previously found to be linearly dependent with the uv power in the range explored here (cf. Fig. 2 of Ref. [17]). It is not clear, however, why there is such good agreement seen between the magnitudes of the other data sets, despite similar decay in laser power between scans.

The widths of the observed resonances are a product of several contributing factors. For excitation to low-n states (i.e., $n < 25$), the breadth of features is primarily due to the bandwidth of the ir laser pulse, while at higher levels, motional Stark splitting of states becomes increasingly important, growing like $n(n - |m| - 1)$ [19]. In the present experiment, the Stark broadening of lines limits resolution of individual n states up to $n \sim 30$.

Near the term limit the observed signal rate, in the absence of an electric field, is expected to converge on a constant value, as a balance is struck between the increasing level density ($\propto n^3$) and the shrinking dipole moment (and hence the excitation cross section $\propto n^{-3}$) of each transition [18]. Approaching the term limit, there is a clear decrease in the observed counts, starting around $n = 50$, with no significant signal observed above $n \approx 100$. This loss in signal is due to the motional electric field experienced by the Rydberg atoms near the Si target becoming sufficient to field ionize the atoms [18,19], and thus preventing their detection.

IV. CONCLUDING REMARKS

We have presented here results of experiments involving preparation of Rydberg Ps, resolved (for principal quantum number n) up to $n \approx 30$, and detected after traveling a distance of 0.56 m. Transmission of Ps atoms over a significant path length is valuable preparation for a proposed Ps gravity experiment [7], providing an indirect measure of the severity of various loss processes, e.g., ionization due to blackbody radiation, loss due to scattering from background gases, and loss in flight due to radiative decay. Production of highly excited Rydberg Ps states is a necessary prerequisite for the efficient production of Rydberg antihydrogen, as proposed by the AEGIS collaboration [9]. The inability of the present experiment to differentiate decay lifetimes indicates that improved counting rates and longer delay times are needed. The results of this experiment confirm the role of the motional Stark effect in limiting the resolution and range of accessible states of earlier experiments, conducted in a strong (~0.16 T) magnetic field [17], as explained by Hogan [18] and reinforces the need for an efficient source of cold Ps. While no ideal material has been discovered, Al(111) treated with oxygen [41] has been used to produce thermal Ps at $\leqslant 100$ K [7,42], although with a significant reduction in the Ps production efficiency, as compared with the present experiment. More recently, porous silica, in the form of bulk aerogel [43] and mesoporous thin films [44], has been demonstrated to efficiently produce cold Ps with minimal loss at cryogenic temperatures.

Position-sensitive observation of Rydberg Ps is performed here to first order by selecting only Ps emitted in a small angular range that travels through the drift tube. This knowledge allows us to correct for the first-order Doppler effect. Using two-dimensional (2D) position-sensitive detection and operating with a pointlike source of Ps, it will be possible to further correct for variations in the first-order Doppler effect, and eventually the second-order Doppler effect. This technique will be critical for making precision measurements of transitions in Ps, for example, in improving the accuracy of measurements of the $1S$-$2S$ transition frequency, by post-excitation production of Rydberg Ps.

Through state-resolved production of Rydberg Ps, spectroscopic measurements of transition line centers are possible. In the present data, measurement of the ir laser wavelength is limited by the the laser bandwidth, limiting the absolute accuracy of these measurements to $\geqslant 50$ GHz. The apparatus described here also makes possible investigation of the energy spectrum of Ps emitted from the target, via TOF spectroscopy. Comparing the TOF spectra from different Rydberg levels, it should be possible to measure the difference in radiative decay rates, however, the present data are insufficient to achieve statistical significance. Improvements to the experiment are planned which will make these measurements easier. First, a pulsed HV accelerator will be installed between the positron trap and the target, to ensure positrons are implanted sufficiently deep into the sample as to properly thermalize. Second, an increase in the flight path will provide a larger scale for determination of the energy spectrum, as well as enhancing the relative impact of loss in flight, making it possible to better measure the Rydberg Ps lifetimes.

In the near future, we plan to investigate the specular reflection of Rydberg Ps from a surface, in the hopes of finding a suitable material from which to construct a focusing mirror, another necessary ingredient for the proposed Ps gravity experiment.

[1] S. G. Karshenboim, Appl. Surf. Sci. **194**, 307 (2002).

[2] S. G. Karshenboim, Phys. Rep. **422**, 1 (2005).

[3] T. S. Pedersen, J. R. Danielson, C. Hugenschmidt, G. Marx, X. Sarasola, F. Schauer, L. Schweikhard, C. M. Surko, and E. Winkler, New J. Phys. **14**, 035010 (2012).

[4] M. S. Fee, S. Chu, A. P. Mills, R. J. Chichester, D. M. Zuckerman, E. D. Shaw, and K. Danzmann, Phys. Rev. A **48**, 192 (1993).

[5] V. Meyer *et al.*, Phys. Rev. Lett. **84**, 1136 (2000).

[6] A. P. Mills, Jr., JPS Conf. Proc. **2**, 010401 (2014).

[7] A. P. Mills, Jr. and M. Leventhal, Nucl. Instrum. Methods Phys. Res., Sect. B **192**, 102 (2002).

[8] M. Charlton, Phys. Lett. A **143**, 143 (1990).

[9] A. Kellerbauer *et al.*, Nucl. Instrum. Methods Phys. Res., Sect. B **266**, 351 (2008).

[10] C. H. Storry, A. Speck, D. Le Sage, N. Guise, G. Gabrielse, D. Grzonka, W. Oelert, G. Schepers, T. Sefzick, H. Pittner, M. Herrmann, J. Walz, T. W. Hänsch, D. Comeau, and E. A. Hessels, Phys. Rev. Lett. **93**, 263401 (2004).

[11] G. F. Gribakin, J. A. Young, and C. M. Surko, Rev. Mod. Phys. **82**, 2557 (2010).

[12] D. M. Schrader, in *Physics with Many Positrons*, edited by A. Dupasquier and A. P. Mills, Jr. (Societá Italliana di Fisica, Varenna, 2010), p. 337.

[13] J. Mitroy, M. W. J. Bromley, and G. G. Ryzhikh, J. Phys. B: At., Mol. Opt. Phys. **35**, R81 (2002).

[14] X. Cheng, D. Babikov, and D. M. Schrader, Phys. Rev. A **83**, 032504 (2011).

[15] X. Cheng, D. Babikov, and D. M. Schrader, Phys. Rev. A **85**, 012503 (2012).

[16] K. P. Ziock, R. H. Howell, F. Magnotta, R. A. Failor, and K. M. Jones, Phys. Rev. Lett. **64**, 2366 (1990).

[17] D. B. Cassidy, T. H. Hisakado, H. W. K. Tom, and A. P. Mills, Jr., Phys. Rev. Lett. **108**, 043401 (2012).

[18] S. D. Hogan, Phys. Rev. A **87**, 063423 (2013).

[19] F. Castelli, Eur. Phys. J. Special Topics **203**, 137 (2012).

[20] D. B. Cassidy, T. H. Hisakado, V. E. Meligne, H. W. K. Tom, and A. P. Mills, Jr., Phys. Rev. A **82**, 052511 (2010).

[21] C. M. Surko and R. G. Greaves, Phys. Plasmas **11**, 2333 (2004).

[22] K. F. Canter, A. P. Mills, Jr., and S. Berko, Phys. Rev. Lett. **34**, 177 (1975).

[23] R. Ley, K. D. Niebling, G. Werth, C. Hahn, H. Schneider, and I. Tobehn, J. Phys. B: At., Mol. Opt. Phys. **23**, 3437 (1990).

[24] D. C. Schoepf, S. Berko, K. F. Canter, and P. Sferlazzo, Phys. Rev. A **45**, 1407 (1992).

[25] T. D. Steiger and R. S. Conti, Phys. Rev. A **45**, 2744 (1992).

[26] D. J. Day, M. Charlton, and G. Laricchia, J. Phys. B: At., Mol. Opt. Phys. **34**, 3617 (2001).

[27] D. B. Cassidy, T. H. Hisakado, H. W. K. Tom, and A. P. Mills, Jr., Phys. Rev. Lett. **106**, 133401 (2011).

[28] D. B. Cassidy, T. H. Hisakado, H. W. K. Tom, and A. P. Mills, Jr., Phys. Rev. B **84**, 195312 (2011).

[29] D. B. Cassidy, T. H. Hisakado, H. W. K. Tom, and A. P. Mills, Jr., Phys. Rev. B **86**, 155303 (2012).

[30] Bristol Inc., "821 series laser wavelength meter", available online http://e-news.bfioptilas.com/e_news/fr/news40/MEAS/bristol821wavelengthmeter.pdf.

[31] M. B. Morris, T. J. McIlrath, and J. J. Snyder, Appl. Opt. **23**, 3862 (1984).

[32] The background subtraction technique used when projecting data by wavelength is not appropriate for correction of the background for TOF distribution data, as artifacts are introduced.

[33] T. F. Gallagher and W. E. Cooke, Phys. Rev. Lett. **42**, 835 (1979).

[34] S. D. Chao, M. Hayashi, S. H. Lin, and E. W. Schlag, J. Chin. Chem. Soc. **45**, 491 (1998).

[35] H. A. Bethe and E. A. Salpeter, *Quantum Mechanics of One- and Two-Electron Atoms* (Springer, Berlin, 1957).

[36] C. B. Tarter, J. Math. Phys. **11**, 3192 (1970).

[37] S. M. Curry and A. L. Schawlow, Phys. Lett. A. **37**, 5 (1971).

[38] D. W. Gidley, P. W. Zitzewitz, K. O. Marko, and A. Rich, Phys. Rev. Lett. **37**, 729 (1976).

[39] P. Sferlazzo, S. Berko, and K. F. Canter, Phys. Rev. B **35**, 5315 (1987).

[40] A. P. Mills, Jr., E. D. Shaw, R. J. Chichester, and D. M. Zuckerman, Phys. Rev. B **40**, 2045 (1989).

[41] K. G. Lynn and H. Lutz, Phys. Rev. B **22**, 4143 (1980).

[42] A. P. Mills, E. D. Shaw, M. Leventhal, R. J. Chichester, and D. M. Zuckerman, Phys. Rev. B **44**, 5791 (1991).

[43] R. Ferragut *et al.*, Can. J. Phys. **89**, 17 (2011).

[44] P. Crivelli, U. Gendotti, A. Rubbia, L. Liszkay, P. Perez, and C. Corbel, Phys. Rev. A **81**, 052703 (2010).